Numerical study on the angular light trapping of the energy yield of organic solar cells with an optical cavity

JONATHAN LEHR,[1,4] ADRIAN MERTENS,[1,2] QUAN LIU,[3] JORDI MARTORELL,[3] ULRICH W. PAETZOLD,[1,2] ⓘD AND ULI LEMMER[1,2,5]

[1]*Light Technology Institute, Karlsruhe Institute of Technology (KIT), Engesserstrasse 13, 76131 Karlsruhe, Germany*
[2]*Institute of Microstructure Technology, Karlsruhe Institute of Technology, Hermann-von-Helmholtz-Platz 1, 76344 Eggenstein-Leopoldshafen, Germany*
[3]*ICFO-Institut de Ciencies Fotoniques, The Barcelona Institute of Science and Technology, 08860 Castelldefels (Barcelona), Spain*
[4]*jonathan.lehr@kit.edu*
[5]*uli.lemmer@kit.edu*

Abstract: A limiting factor in organic solar cells (OSCs) is the incomplete absorption in the thin absorber layer. One concept to enhance absorption is to apply an optical cavity design. In this study, the performance of an OSC with cavity is evaluated. By means of a comprehensive energy yield (EY) model, the improvement is demonstrated by applying realistic sky irradiance, covering a wide range of incidence angles. The relative enhancement in EY for different locations is found to be 11-14% compared to the reference device with an indium tin oxide front electrode. The study highlights the improved angular light absorption as well as the angular robustness of an OSC with cavity.

1. Introduction

Organic photovoltaics (OPV) offers a low-cost alternative to silicon (Si) photovoltaics (PV) by utilizing abundant materials and featuring mechanical flexibility and simple fabrication techniques [1–3]. Particularly, the case of building integrated PV (BIPV) and energy harvesting in wearables is a potential future field of application for OPV. In an organic solar cell (OSC), the thickness of the bulk heterojunction is very limited by low charge carrier mobilities and relatively high recombination rates. Thin layers show an enhanced charge carrier collection efficiency but compromise the light absorption. Thus, many light management concepts have been applied for improving the light trapping in OSC [4]. The absorption can, e.g., be enhanced by scattering light at dielectric nanoparticles [5], by inducing plasmon resonances due to nanostructured metallic electrodes [6,7] and nanoparticles [8,9], by inserting one-dimensional photonic crystals [10,11]. A particularly interesting concept enabled by the very thin absorber layers is the use of an optical cavity [12–14]. An optical cavity can easily be realized by an absorber layer surrounded by two metallic electrodes forming a resonator. For this, the front electrode in an OSC, which is commonly indium-tin oxide (ITO), is replaced by a thin metallic layer. Liu *et al.* have recently shown the improvement in light absorption by amplifying optical modes with a cavity configuration resulting in a broadband light trapping [15]. The concept was already applied to organic three-terminal (3 T) tandem solar cells [16]. However, the investigation of the light trapping effect and the corresponding increase in absorption was only performed for normal incidence of light so far, even though the interdependency is not trivial for angular light

incidence. The existent numerical studies deal with the particular case of standard test conditions (STC). Commonly, the short-circuit current density (J_{SC}) is estimated via optical modelling of the device [12,17]. The maximal efficiency gain of a solar cell with cavity configuration was investigated by optimizing the layer stack and comparing it to a conventional OSC containing an ITO front electrode [13,18]. Recently, the potential enhancement of the cavity design was calculated for an organic 3 T solar cell by inserting two additional thin metallic layers, one as front and one as central electrode [19].

By means of energy yield (EY) modelling, the solar cells power output is calculated for realistic outdoor conditions [20,21]. For this purpose, EY modelling usually considers the spectral and temporal sky irradiance and the electrical as well as the optical properties of the device [22]. In particular, EY modelling requires the evaluation of the angular light absorption in the layer stack in order to determine the absorbed power from the directional irradiation. This enables the consideration of both, the direct and diffuse irradiance. Herein, for the direct irradiance, the change in position of the sun during the course of a day is included. For the diffuse irradiance, the angle dependent contributions to the irradiance over all angles of incidence are integrated. The EY is then determined as the annual power output originating from the direct and diffuse sky irradiance impinging from all over the hemisphere on the solar cell. With our in-house developed simulation platform, various single-junction (SJ) and tandem PV modules based on crystalline Si, copper indium gallium diselenide (CIGS), and Perovskite were studied before [23–25].

One possible field of application of OSCs are building facades and windows. Owing to the fixed integration of BIPV, tracking the sun is not feasible. Therefore, effective light trapping in an OSC over a wide range of incidence angles is of key importance for high EY. The increase in light absorption for an OSC with a cavity depends essentially on the design of the solar cell. The layer stack and the dimension of the layers have to be carefully selected in order to reach maximum EY. Furthermore, it has to be clarified, if the cavity design is also advantageous for arbitrary angles of incidence, since the light trapping effect owing to constructive light interference may be detrimental under oblique light incidence. Hence, the intention of this study is also to analyze the performance of a cavity configuration under oblique incidence angle and to check if an optimized architecture for normal incidence has negative effects on the light trapping under oblique incidence angles compared to a conventional design.

2. Results and discussion

With the integration of a thin metallic electrode at the front side of an OSC, a distinct enhancement in light absorption over a broad spectral range is achievable. As starting point, the light trapping is analyzed for a solar cell architecture with cavity resonator for normal light incidence. An in-house simulation framework is used, which is subsequently applied to determine the EY under realistic irradiance conditions as well. The calculation of EY is based on the optical and electrical properties of the organic SJ solar cell. A transfer-matrix method is used to calculate the spectral absorptance, reflectance and transmittance of the thin film solar cell. By employing Fresnel equations, the optics of the layer stack are determined for arbitrary incidence angle [26]. The glass substrate with a thickness in the range of millimeters is treated as optically thick and thus the light propagation in this layer is calculated by applying a series expansion onto the Beer-Lambert law [22]. The electrical properties of the device are described by applying a one-diode model based on the Shockley equation [22,27].

The investigated OSC is based on a poly[4,8-bis(5-(2-ethylhexyl)thiophen-2-yl)benzo[1,2-b;4,5-b']dithiophene-2,6-diyl-alt-(4-(2-ethylhexyl)-3-fluorothieno[3,4-b]thiophene)-2-carboxylate-2-6-diyl] (PTB7-Th):[6,6]-phenyl C71 butyric acid methyl ester ($PC_{71}BM$) absorber layer. The architecture is inspired by Liu *et al.* [15] and exhibits a cavity, which basically forms two fundamental resonances. A schematic of the layer stacks for the cavity OSC and for the conventional OSC without cavity as reference are shown in Fig. 1(a). The front electrode of the reference

consists of ITO (70 nm) on top of a glass substrate (1 mm). In order to reduce reflection losses, a magnesium fluoride (MgF$_2$) layer (90 nm) is used as anti-reflection coating (ARC) on the front side of the substrate. The architecture of the cavity OSC uses silver (Ag) as front electrode with a thickness of 8 nm (see Fig. 1(a)) as well as an ARC with adapted layer thickness (100 nm). The front electrode is covered with zinc oxide (ZnO) layers at both sides of the thin Ag layer for improving the quality and electrical properties of the front contact, as reported by Liu *et al.* [15]. The rear side of the solar cell consists of a molybdenum trioxide (MoO$_3$) layer (5 nm) and Ag electrode (100 nm). Similar to a cavity, the metallic front and rear electrodes form a resonance in the absorber layer corresponding to a wavelength of ~655 nm. A dielectric titanium dioxide (TiO$_2$) layer (35 nm) in front of the thin Ag electrode enables a second resonance with a corresponding wavelength of ~425 nm. The origin of the second resonance is different, since here the arising standing wave has an open-end boundary condition at the side of the dielectric layer. Figure 1(b) shows the intensity of the electrical field under normal light incidence across the thin film layer stack of the cavity OSC for two configurations, i) for a 15 nm Ag front electrode, and ii) without Ag front electrode. In case i), the intensity is increased for wavelengths at around 655 nm, and in case ii) at around 425 nm.
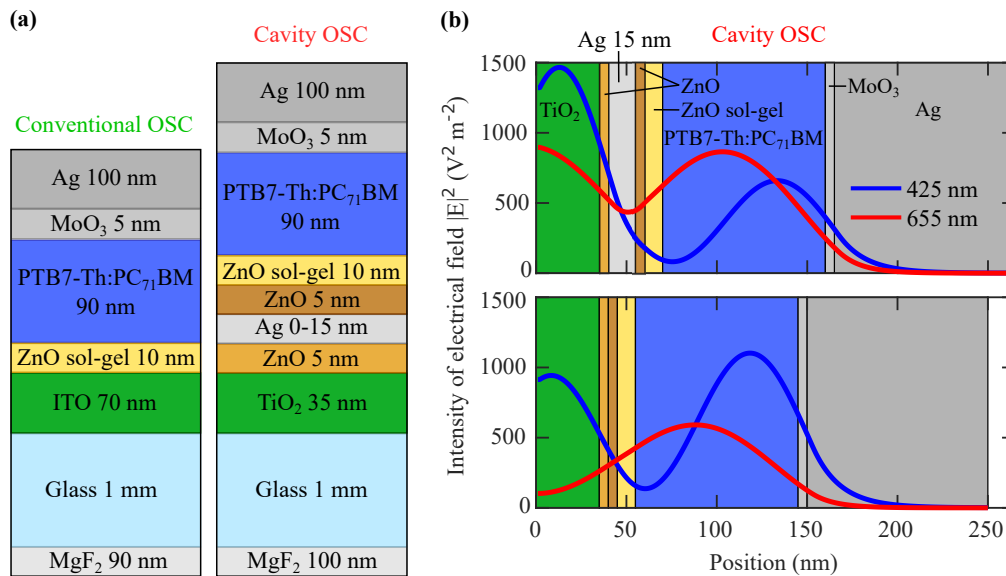

Fig. 1. (a) Architectures of the conventional OSC without cavity (left) as well as the cavity OSC (right). (b) Intensity of the electrical field as a function of the position for the cavity OSC in two configurations, with 15 nm Ag front electrode (top) and without Ag front electrode (bottom). The intensity is shown for the wavelengths 425 nm and 655 nm.

For calculating the EY later, we briefly discuss the electrical model of the solar cells. The calculation of the current-density versus voltage (*J-V*) characteristics is based on the electrical parameters dark saturation current density J_0, ideality factor n and series resistance R_S. The open-circuit voltage (V_{OC}) of the solar cell is calculated by applying the Shockley equation. Herein, the implicit equation for the V_{OC} is solved by using the Lambert W function [28], as detailed described in Schmager *et al.* [22]. The fill factor (FF) and the power conversion efficiency (PCE) are calculated by determining the maximal power point of the obtained *J-V* characteristics. The set of electrical parameters used for the conventional OSC as reference is $J_0 = 3.5 \times 10^{-11}$ mA cm^{-2}, n = 1.2, and $R_S = 7.7$ Ω and for the cavity OSC $J_0 = 3 \times 10^{-8}$ mA

cm^{-2}, n = 1.6, and R_S = 3.9 Ω. The metallic front electrode shows a low sheet resistance, which is reduced by a factor of 2 compared to the R_S of the conventional device. This results in a higher fill factor (FF) of the cavity OSC as an additional positive effect. Furthermore, a charge carrier collection efficiency of 90% [29] is applied, in order to account for recombination losses. The corresponding *J-V* characteristics are presented in the Fig. S1 (see Supplement 1) and mimic the electrical properties of the devices from Liu *et al.* [15].

The spectral absorptance in each layer under normal light incidence is shown in Fig. 2 for both, the conventional OSC and the cavity OSC. Here, the architecture of the cavity OSC was optimized for a PTB7-Th:PC$_{71}$BM absorber layer thickness of 90 nm and for illumination with the air-mass 1.5 global (AM1.5 g) spectrum, in accordance to the STC. Accordingly, the absorptance of the conventional OSC is shown for the same absorber layer thickness of PTB7-Th:PC$_{71}$BM. The thicknesses of the other layers are optimized for maximal light absorption and are given in Fig. 1. With the enhanced overall absorptance in the PTB7-Th:PC$_{71}$BM, the cavity OSC clearly outperforms the reference. The absorptance spectra of PTB7-Th:PC$_{71}$BM in both devices are also directly compared in Fig. S2 (see Supplement 1). The increase in light absorption originates from the interaction of both resonances (see Fig. 1(b)) and results in an enhancement over a broad spectral range. By tuning the thickness of the Ag front electrode to 8 nm, the strength of both resonances is balanced in order to maximize the overall absorptance in the PTB7-Th:PC$_{71}$BM layer. The overall enhancement in light absorption is reduced for wavelengths < 400 nm owing to parasitic absorption in the dielectric TiO$_2$ layer and the ZnO layers. Though, for the realization of the resonator architecture all these layers are required and the applied materials were already carefully selected [15]. In summary, for the presented layer stacks, the integrated J_{SC} for the incident AM1.5 g spectrum is increased from 16.8 mA cm^{-2} (conventional OSC) to 18.7 mA cm^{-2} (cavity OSC), as shown in Fig. 2.
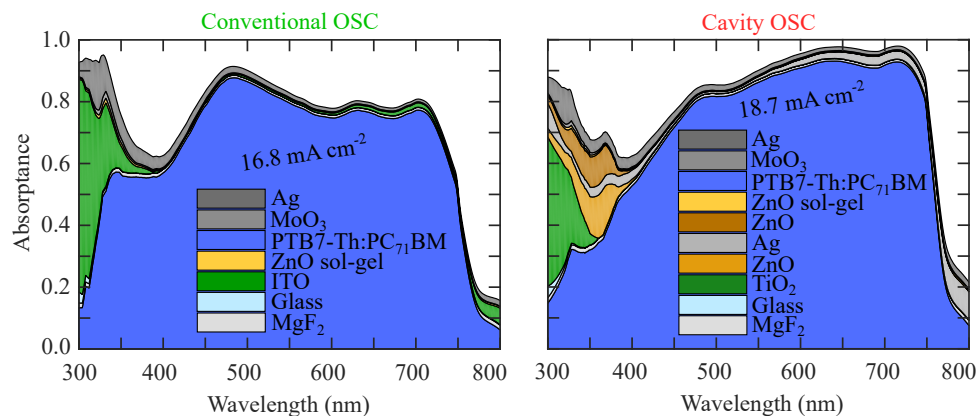
Fig. 2. Absorptance spectra of the conventional OSC as well as the cavity OSC with a PTB7-Th:PC$_{71}$BM absorber layer thickness of 90 nm under normal light incidence. The integrated J_{SC} at an illumination with AM1.5 g is indicated for the absorber layer. For the calculation of the J_{SC}, a collection efficiency of 90% owing to charge carrier recombination is assumed.

In order to demonstrate the mechanism of light absorption by utilizing resonant modes, the number of absorbed photons under AM1.5 g irradiation is shown in Fig. 3 as a function of the PTB7-Th:PC$_{71}$BM absorber layer thickness. Obviously, the improved light trapping for the cavity OSC requires a well designed layer configuration and is only limited to a small interval of absorber layer thickness. Since the charge transport is limited due to charge carrier recombination, the thickness of the PTB7-Th:PC$_{71}$BM layer is usually about 100 nm [30]. As shown in Fig. 3,

increasing the layer thickness enhances the light absorption in both devices. However, the thicker organic bulk heterojunctions (see shaded area in Fig. 3) are less efficient owing to the increased recombination losses [31]. The calculated maximal enhancement in absorbed photons is 11% relative for the cavity OSC. Accordingly, the J_{SC} increases by 11% relative. Owing to the low R_S of the metallic front electrode, the PCE of 11.0% is actually enhanced by 17% relative to the value of 9.4% of the reference with ITO (see Supplement 1, Fig. S1). Overall, the comparison shows the advantage of a cavity OSC under *normal* light incidence.
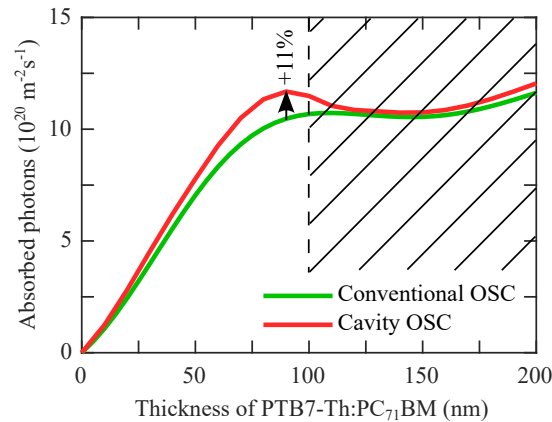
Fig. 3. Calculated number of absorbed photons as a function of the PTB7-Th:PC$_{71}$BM absorber layer thickness for the cavity OSC as well as the reference. For the cavity OSC, the dielectric layer TiO$_2$ and the Ag front electrode are optimized at each absorber layer thickness. The solar cells are illuminated with an AM1.5 g spectrum under normal light incidence, according to STC. The shaded area is not accessible due to the strong increase in recombination losses in thick absorber layers.

Featuring reliable device performance under realistic irradiance conditions requires an improved light absorption for a wide range of incidence angles. Most of the light impinges on the solar cell under inclined angle, owing to the change in position of the sun as well as due to the wide distribution of diffuse radiation from the sky. The discussed layer stack of the cavity OSC was designed in order to enhance the absorption of light with normal incidence. Since the spectrally dependent interference patterns change for oblique incidence angles, the light trapping effect is expected to be suppressed for different angles of incidence or can even turn into a detrimental effect. In the following, we analyze the overall effect of light interference for oblique angle of incidence. In Fig. 4, the calculated effective J_{SC} (J_{SC}*) is shown as a function of incidence angles under illumination with the AM1.5 g spectrum. The calculation is performed for each angle individually considering an AM1.5 g spectrum. Both devices feature a PTB7-Th:PC$_{71}$BM absorber layer thickness of 90 nm. The J_{SC}* accounts for the change in the effective area of the solar cell under oblique angle. Hence, the J_{SC} is divided by the cosine of the incidence angle, in order to account for the reduced effective area. The cavity OSC shows an improved J_{SC} for the complete range of incidence angles compared to the reference (see Fig. 4). From the value of 11% relative for normal light incidence, the enhancement persists above 6% relative over the whole range of incidence angles. This implies an apparent higher light absorption of both, the incident diffuse and direct irradiance under real conditions. There is no disadvantageous effect on the angular light trapping observed for a cavity OSC. Even though the effective resonator length of the device changes with incidence angle, owing to the light interference effect over a broad spectral range, an overall enhanced light trapping in the cavity is prevalent.
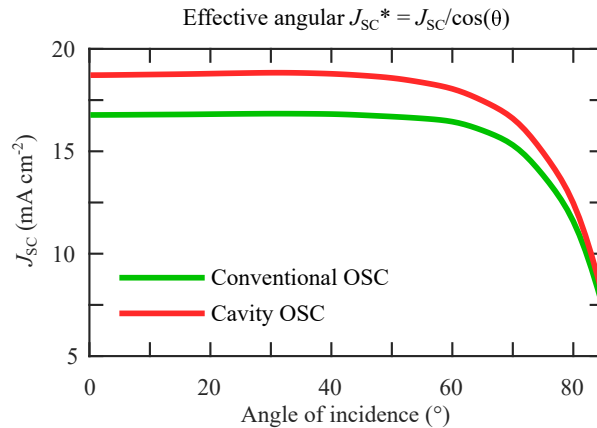
Fig. 4. Simulation of the generated J_{SC} in both devices by illumination with an AM1.5 g spectrum for arbitrary incidence angle. The $J_{SC}*$ (effective J_{SC}) is shown in order to account for the change in effective device area for oblique incidence angle. The used PTB7-Th:PC$_{71}$BM absorber layer thickness is 90 nm.

Next, the performance of the solar cells is evaluated under realistic irradiance conditions. In order to represent different climate conditions, we choose the locations Detroit (Michigan) with a humid continental climate, Miami (Florida) with tropical monsoon climate, Nashville (Tennessee) with humid subtropical climate, Phoenix (Arizona) with hot desert climate, and Portland (Oregon) with temperate warm-summer climate [32]. In Fig. 5(a), the calculated EY for the cavity OSC and for the reference device is presented. At every location, the device is exposed to different irradiance conditions with regard to the incidence angle, the spectrum and the intensity of the direct and diffuse irradiance. Since the cavity OSC shows a superior light absorption for all incidence angles, this results in an enhanced EY at every location. E.g., in Phoenix, the calculated EY is 250 kW h m^{-2} a^{-1} for the reference device and 285 kW h m^{-2} a^{-1} for the cavity OSC. Overall, the cavity OSC shows in all cases a relative enhancement of 11-14% in EY compared to the reference. Variations originate from the diverse climate conditions, resulting in different ratios of direct and diffuse irradiance as well as different incident angles. Overall, the relative increase under realistic irradiance conditions is lower than under STC with the very specific normal irradiance. However, the increase in EY under real world conditions is still significant, showing the advantage of applying the cavity configuration to OSCs. In order to maximize the EY, the tilt angle of the device was optimized for every location. The optimal tilt angle is close to the latitude of the location. In this calculation, the rotation angle of the solar cell is kept constant southward.

In order to analyze the influence of the solar cell orientation under realistic irradiance conditions, the EY is calculated for arbitrary tilt and arbitrary rotation in the range of East (E) over South (S) to West (W). In Fig. 5(b, c), we present the EY of the conventional OSC and the cavity OSC for the location Phoenix with respect to the specified range of orientations. As expected, the optimal rotation angle is found close to southwards. Furthermore, the cavity OSC features a high EY for a wide range of orientations. As depicted in Fig. 5(c), the confidence interval for 95% of the maximal EY includes a large range of tilt angles as well as rotation angles ranging from 7° to 45° and 126° to 227°, respectively. Hence, the solar cell exhibits a good angular stability and is as robust as the reference device.

So far, the enhancement in EY of a cavity OSC was evaluated for a device architecture with a layer stack optimized for normal incidence. However, for oblique light incidence, the

(a)

(b) Phoenix, Conventional OSC

(c) Phoenix, Cavity OSC
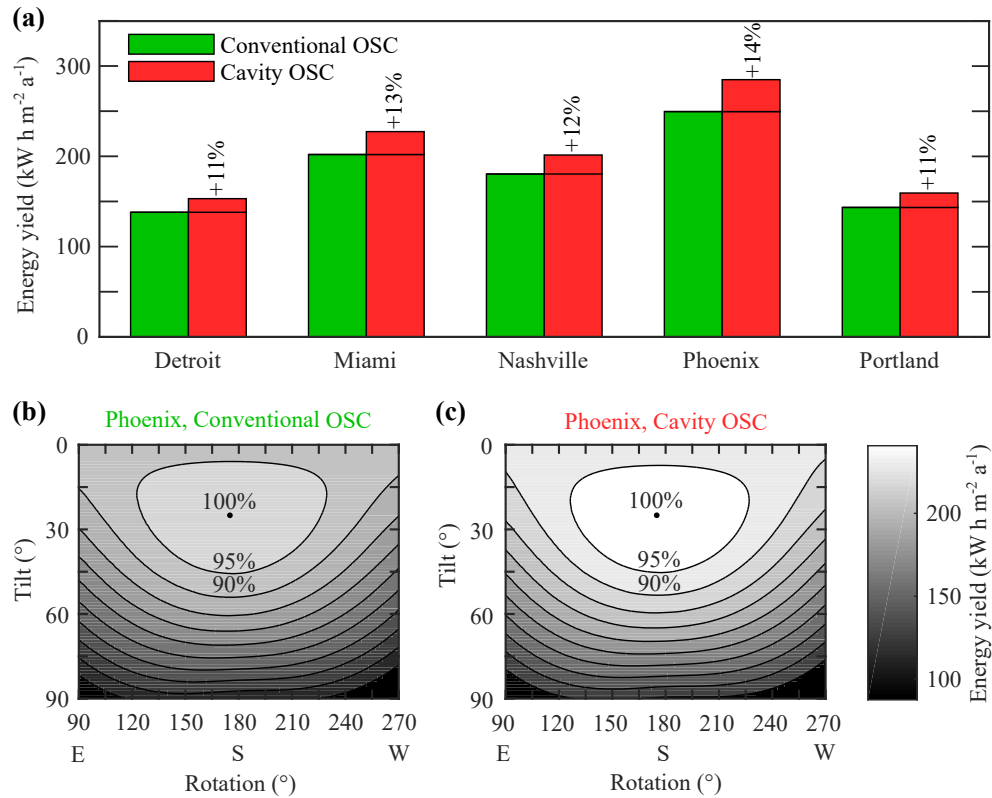
Fig. 5. (a) EY of the cavity OSC and the reference for the locations Detroit (Michigan), Miami (Florida), Nashville (Tennessee), Phoenix (Arizona), and Portland (Oregon). The calculation is performed for the PTB7-Th:PC$_{71}$BM absorber layer thickness of 90 nm as well as for the optimal tilt angle at every location. The relative enhancement in EY for the cavity OSC is indicated for every location. (b, c) EY of the conventional OSC and the cavity OSC as a function of the tilt angle as well as the rotation angle.

enhancement based on this reference architecture is not the optimum. If the solar cell is installed with an unoptimized orientation as it occurs, e.g., for BIPV, and thus the main part of light impinges under oblique incidence angle, the resulting performance can be improved. In most of the cases, the maximal direct radiation from the sun at noon does not hit the solar cell with normal incidence. Therefore, the layer stack has to be adapted to the corresponding incidence angle for the given installation of the solar cell. In order to assess the maximal accessible gain, an optimization of the optical resonator structure was performed for the PTB7-Th:PC$_{71}$BM absorber layer thickness of 90 nm. For every integer angle from 0° to 85°, the optimal configuration was evaluated by optimizing the layers (i) thin Ag front electrode (5-15 nm), (ii) dielectric layer TiO$_2$ (10-40 nm), and (iii) ARC (90-150 nm). The original architecture is then compared to the optimized architecture in Fig. 6. Here, the device is again illuminated with the AM1.5 g spectrum for every angle of incidence, as in Fig. 4. Accordingly, the performance can be further improved by optimizing the layer stack with respect to the incidence angle. Table 1 shows the resulting optimized parameters of the device architecture for certain incidence angles. Overall, however, the additional relative enhancement is limited and amounts to 4% in J_{SC} compared to the reference architecture for one specific angle.
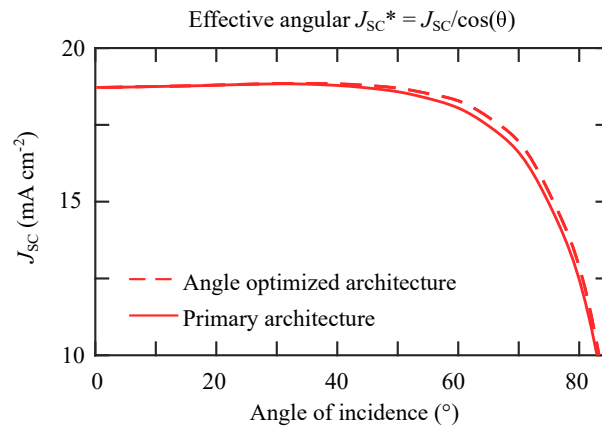
Fig. 6. Calculated $J_{SC}*$ as function of the incidence angle for different architectures of the cavity OSC. The angle optimized architecture shows the maximal possible $J_{SC}*$ with an optimized layer stack for every single incidence angle. The primary architecture shows the $J_{SC}*$ of the original architecture, which is optimized for maximal performance under normal light incidence.

Table 1. Calculated optimal parameters for the layers Ag front electrode, TiO$_2$, and ARC of the cavity OSC. The optimization is performed in order to maximize the light absorption under oblique incidence angles.

Angle of incidence (°)	Thickness of front Ag (nm)	Thickness of TiO$_2$ (nm)	Thickness of ARC (nm)
20	8	32	102
40	7	28	106
60	6	24	122
80	5	16	142

The results for the cavity OSC under the very specific STC are in accordance with other findings. With the concept of an optical cavity, actually OSCs with a PCE of 14% were achieved, enhancing the PCE by 13% relative compared to a reference with ITO front electrode [14]. Liu *et al.* showed a similar enhancement of 14% relative in PCE [15]. Due to the high electrical conductivity of the Ag front electrode, this concept shows an additional advantage against other concepts, for instance the integration of one-dimensional photonic crystals as Bragg reflector into semitransparent OSCs, showing a relative increase of 9% in PCE [11]. Hence, we attribute a high potential to the concept of an optical cavity, to further enhance the performance of state-of-the-art OSCs with a current PCE of 17.3% [33]. The application in organic tandem solar cells with multiple thin metal electrodes is more complex but also promising and could be a subject to future investigations. Though, the optimization will take a higher effort. The incident light spectrum varies for locations with different shares of direct and diffuse irradiance. Thus, the EY model also offers the ability to study the influence of the spectral irradiance on the optimal bandgap of organic absorbers in multi-junction solar cells under real world conditions. The model can also be applied to evaluate the EY of semitransparent OSCs.

3. Conclusion

We have studied the suitability of an optical resonator architecture for enhancing the power output of an OSC under realistic outdoor conditions. The gain in light absorption over a broad spectral range, due to the formation of resonant modes, is not limited to the very specific case

of normal light incidence. Owing to the overall gain in angular light absorption, an OSC with optical cavity outperforms also for arbitrary incidence angle the conventional design with an ITO front electrode. By means of EY modelling, the power output was estimated for various locations covering different climatic conditions. The resulting gain is attributed to the enhanced light trapping and further to a reduced R_S due to the thin metallic front electrode. Whereas for normal light incidence, the relative enhancement in PCE is 17%, the relative increase in EY is determined to 11-14%. The small decrease in EY compared to STC is explained by the distribution of direct and diffuse irradiance across the sky and by less efficient but still superior angular light absorption in the cavity OSC. Furthermore, the cavity configuration shows a good angular robustness over a wide range of solar cell orientations, even though the layer stack was designed for optimal performance under normal light incidence. It was shown, that the concept of an optical cavity does not only enhance the PCE under STC, but is also suitable for realistic conditions. These findings highlight the potential of the cavity concept to further enhance the EY of state-of-the-art OSCs.

Funding

Disclosures

The authors declare no conflicts of interest.

See Supplement 1 for supporting content.

References

1. J. Peet, A. J. Heeger, and G. C. Bazan, ""Plastic" Solar Cells: Self-Assembly of Bulk Heterojunction Nanomaterials by Spontaneous Phase Separation," Acc. Chem. Res. **42**(11), 1700–1708 (2009).
2. G. Li, R. Zhu, and Y. Yang, "Polymer solar cells," Nat. Photonics **6**(3), 153–161 (2012).
3. Q. Wang, Y. Xie, F. Soltani-Kordshuli, and M. Eslamian, "Progress in emerging solution-processed thin film solar cells - Part I: Polymer solar cells," Renewable Sustainable Energy Rev. **56**, 347–361 (2016).
4. Q.-D. Ou, Y.-Q. Li, and J.-X. Tang, "Light Manipulation in Organic Photovoltaics," Adv. Sci. **3**(7), 1600123 (2016).
5. H.-W. Chang, J. Lee, S. Hofmann, Y. H. Kim, L. Müller-Meskamp, B. Lüssem, C.-C. Wu, K. Leo, and M. C. Gather, "Nano-particle based scattering layers for optical efficiency enhancement of organic light-emitting diodes and organic solar cells," J. Appl. Phys. **113**(20), 204502 (2013).
6. J. You, X. Li, F. Xie, W. E. I. Sha, J. H. W. Kwong, G. Li, W. C. H. Choy, and Y. Yang, "Surface Plasmon and Scattering-Enhanced Low-Bandgap Polymer Solar Cell by a Metal Grating Back Electrode," Adv. Energy Mater. **2**(10), 1203–1207 (2012).
7. X. Li, W. C. H. Choy, X. Ren, J. Xin, P. Lin, and D. C. W. Leung, "Polarization-independent efficiency enhancement of organic solar cells by using 3-dimensional plasmonic electrode," Appl. Phys. Lett. **102**(15), 153304 (2013).
8. H. A. Atwater and A. Polman, "Plasmonics for improved photovoltaic devices Harry A," Nat. Mater. **9**(3), 205–213 (2010).
9. K. R. Catchpole and A. Polman, "Plasmonic solar cells," Opt. Express **16**(26), 21793–21800 (2008).
10. R. Betancur, P. Romero-Gomez, A. Martinez-Otero, X. Elias, M. Maymó, and J. Martorell, "Transparent polymer solar cells employing a layered light-trapping architecture," Nat. Photonics **7**(12), 995–1000 (2013).
11. W. Yu, X. Jia, Y. Long, L. Shen, Y. Liu, W. Guo, and S. Ruan, "Highly Efficient Semitransparent Polymer Solar Cells with Color Rendering Index Approaching 100 Using One-Dimensional Photonic Crystal," ACS Appl. Mater. Interfaces **7**(18), 9920–9928 (2015).
12. N. P. Sergeant, A. Hadipour, B. Niesen, D. Cheyns, P. Heremans, P. Peumans, and B. P. Rand, "Design of Transparent Anodes for Resonant Cavity Enhanced Light Harvesting in Organic Solar Cells," Adv. Mater. **24**(6), 728–732 (2012).
13. K.-D. Kim, T. Pfadler, E. Zimmermann, Y. Feng, J. A. Dorman, J. Weickert, and L. Schmidt-Mende, "Decoupling optical and electronic optimization of organic solar cells using high-performance temperature-stable TiO2/Ag/TiO2 electrodes," APL Mater. **3**(10), 106105 (2015).

14. Q. Liu, J. Toudert, T. Li, M. Kramarenko, G. Martínez-Denegri, L. Ciammaruchi, X. Zhan, and J. Martorell, "Inverse Optical Cavity Design for Ultrabroadband Light Absorption Beyond the Conventional Limit in Low-Bandgap Nonfullerene Acceptor–Based Solar Cells," Adv. Energy Mater. **9**(20), 1–8 (2019).

15. Q. Liu, P. Romero-Gomez, P. Mantilla-Perez, S. Colodrero, J. Toudert, and J. Martorell, "A Two-Resonance Tapping Cavity for an Optimal Light Trapping in Thin-Film Solar Cells," Adv. Energy Mater. **7**(18), 1–8 (2017).

16. L. Zuo, C.-C. Chueh, Y.-X. Xu, K.-S. Chen, Y. Zang, C.-Z. Li, H. Chen, and A. K. Y. Jen, "Microcavity-Enhanced Light-Trapping for Highly Efficient Organic Parallel Tandem Solar Cells," Adv. Mater. **26**(39), 6778–6784 (2014).

17. J. Lee, S.-Y. Kim, C. Kim, and J.-J. Kim, "Enhancement of the short circuit current in organic photovoltaic devices with microcavity structures," Appl. Phys. Lett. **97**(8), 083306 (2010).

18. Y. Long, "Improving optical performance of inverted organic solar cells by microcavity effect," Appl. Phys. Lett. **95**(19), 193301 (2009).

19. B. Godefroid and G. Kozyreff, "Photonic enhancement of parallel homo-tandem solar cells through the central electrode," Sol. Energy Mater. Sol. Cells **193**, 73–79 (2019).

20. O. Dupré, B. Niesen, S. De Wolf, and C. Ballif, "Field Performance versus Standard Test Condition Efficiency of Tandem Solar Cells and the Singular Case of Perovskites/Silicon Devices," J. Phys. Chem. Lett. **9**(2), 446–458 (2018).

21. N. Tucher, O. Höhn, J. N. Murthy, J. C. Martinez, M. Steiner, A. Armbruster, E. Lorenz, B. Bläsi, and J. C. Goldschmidt, "Energy yield analysis of textured perovskite silicon tandem solar cells and modules," Opt. Express **27**(20), A1419–A1430 (2019).

22. R. Schmager, M. Langenhorst, J. Lehr, U. Lemmer, B. S. Richards, and U. W. Paetzold, "Methodology of energy yield modelling of perovskite-based multi-junction photovoltaics," Opt. Express **27**(8), A507–523 (2019).

23. J. Lehr, M. Langenhorst, R. Schmager, S. Kirner, U. Lemmer, B. S. Richards, C. Case, and U. W. Paetzold, "Energy yield modelling of perovskite/silicon two-terminal tandem PV modules with flat and textured interfaces," Sustainable Energy Fuels **2**(12), 2754–2761 (2018).

24. M. Langenhorst, B. Sautter, R. Schmager, J. Lehr, E. Ahlswede, M. Powalla, U. Lemmer, B. S. Richards, and U. W. Paetzold, "Energy yield of all thin-film perovskite/CIGS tandem solar modules," Prog. Photovoltaics **27**(4), 290–298 (2019).

25. J. Lehr, M. Langenhorst, R. Schmager, F. Gota, S. Kirner, U. Lemmer, B. S. Richards, C. Case, and U. W. Paetzold, "Energy yield of bifacial textured perovskite/silicon tandem photovoltaic modules," Sol. Energy Mater. Sol. Cells **208**, 110367 (2020).

26. S. J. Byrnes, "Multilayer optical calculations," 1–20 (2019).

27. A. Foertig, J. Rauh, V. Dyakonov, and C. Deibel, "Shockley equation parameters of P3HT:PCBM solar cells determined by transient techniques," Phys. Rev. B: Condens. Matter Mater. Phys. **86**(11), 115302 (2012).

28. A. Jain and A. Kapoor, "Exact analytical solutions of the parameters of real solar cells using Lambert W-function," Sol. Energy Mater. Sol. Cells **81**(2), 269–277 (2004).

29. Y. Liang, Z. Xu, J. Xia, S.-T. Tsai, Y. Wu, G. Li, C. Ray, and L. Yu, "For The Bright Future - Bulk Heterojunction Polymer Solar Cells with Power Conversion Efficiency of 7.4%," Adv. Mater. **22**(20), E135–E138 (2010).

30. Q. Wan, X. Guo, Z. Wang, W. Li, B. Guo, W. Ma, M. Zhang, and Y. Li, "10.8% Efficiency Polymer Solar Cells Based on PTB7-Th and PC71BM via Binary Solvent Additives Treatment," Adv. Funct. Mater. **26**(36), 6635–6640 (2016).

31. A. Guerrero, N. F. Montcada, J. Ajuria, I. Etxebarria, R. Pacios, G. Garcia-Belmonte, and E. Palomares, "Charge carrier transport and contact selectivity limit the operation of PTB7-based organic solar cells of varying active layer thickness," J. Mater. Chem. A **1**(39), 12345–12354 (2013).

32. H. E. Beck, N. E. Zimmermann, T. R. McVicar, N. Vergopolan, A. Berg, and E. F. Wood, "Present and future Köppen-Geiger climate classification maps at 1-km resolution," Sci. Data **5**(1), 180214 (2018).

33. L. Liu, Y. Kan, K. Gao, J. Wang, M. Zhao, H. Chen, C. Zhao, T. Jiu, A.-K.-Y. Jen, and Y. Li, "Graphdiyne Derivative as Multifunctional Solid Additive in Binary Organic Solar Cells with 17.3% Efficiency and High Reproductivity," Adv. Mater. **32**(11), 1–7 (2020).